Methods and Applications in Fluorescence

OPEN ACCESS

RECEIVED
25 September 2019

REVISED
10 March 2020

ACCEPTED FOR PUBLICATION
31 March 2020

PUBLISHED
14 April 2020



PAPER

# A rapid analysis platform for investigating the cellular locations of bacteria using two-photon fluorescence lifetime imaging microscopy

**Natakorn Sapermsap[1], David Day-Uei Li[2,4], Ryath Al-Hemedawi[2], Yahui Li[2,3], Jun Yu[2], David JS Birch[1] and Yu Chen[1]**

[1] Department of Physics, SUPA, University of Strathclyde, John Anderson Building, 107 Rottenrow, Glasgow, G4 0NG, United Kingdom
[2] Strathclyde Institute of Pharmacy and Biomedical Sciences, University of Strathclyde, Glasgow G4 0RE, United Kingdom
[3] Xi'an Institute of Optics and Precision Mechanics, Xi'an, Shanxi 710049, People's Republic of China
[4] Author to whom any correspondence should be addressed.

**E-mail:** natakorn.sapermsap@strath.ac.uk, David.Li@strath.ac.uk and y.chen@strath.ac.uk

**Keywords:** fluorescence lifetime, FLIM, two-photon excitation

## Abstract

Facultative intracellular pathogens are able to live inside and outside host cells. It is highly desirable to differentiate their cellular locations for the purposes of fundamental research and clinical applications. In this work, we developed a novel analysis platform that allows users to choose two analysis models: amplitude weighted lifetime ($\tau_A$) and intensity weighted lifetime ($\tau_I$) for fluorescence lifetime imaging microscopy (FLIM). We applied these two models to analyse FLIM images of mouse Raw macrophage cells that were infected with bacteria *Shigella Sonnei*, adherent and invasive *E. coli* (AIEC) and *Lactobacillus*. The results show that the fluorescence lifetimes of bacteria depend on their cellular locations. The $\tau_A$ model is superior in visually differentiating bacteria that are in extra- and intracellular and membrane-bounded locations, whereas the $\tau_I$ model show excellent precision. Both models show speedy performances that analysis can be performed within 0.3 s. We also compared the proposed models with a widely used commercial software tool ($\tau_C$, SPC Image, Becker & Hickl GmbH), showing similar $\tau_I$ and $\tau_C$ results. The platform also allows users to perform phasor analysis with great flexibility to pinpoint the regions of interest from lifetime images as well as phasor plots. This platform holds the disruptive potential of replacing z-stack imaging for identifying intracellular bacteria.

## 1. Introduction

Fluorescence lifetime imaging microscopy (FLIM) has been developed for detecting bacterial infections in clinical applications. Many imaging methods are dependent on fluorophore-labelled tracers that interact with bacterial surface structural components such as lipopolysaccharide or bacteria enzymes/proteins such as $\beta$-lactamase [1]. On the other hand, bacterial intrinsic fluorescent molecules have also been exploited for detection, such as porphyrins, a red-fluorescent by-product of bacterial haem production, and cyan-fluorescing pyoverdines, which are fluorophores specific to *Pseudomonads* [2]. Most interestingly, two-photon FLIM imaging of the metabolic coenzymes reduced nicotinamide adenine dinucleotides [NAD(P)H] has been used for a separate analysis of host and pathogen metabolisms during intracellular chlamydial infections [3]. More recently, FLIM of [NAD(P)H] has been used for bacterial metabolic fingerprinting in diverse culture conditions [4]. In some cases, autofluorescence from lung tissue spectrally overlaps with signals from labelled bacteria, whereas lifetime images in general give excellent contrast [5]. By applying the phasor approach, this study has generated FLIM-phasor maps for *Escherichia coli*, *Salmonella enterica serovar* Typhimurium, *Pseudomonas aeruginosa*, *Bacillus subtilis*, and *Staphylococcus epidermidis* at the single cell and population levels. In contrast to the *Chlamydia trachomatis,* which is an obligation intracellular pathogen, facultative intracellular pathogens such as *Salmonella*, *Shigella* and pathogenic *E. coli* are able to survive and proliferate inside and outside the host cells. To differentiate intracellular and extracellular bacteria, z-stack imaging is usually required. This technique generates

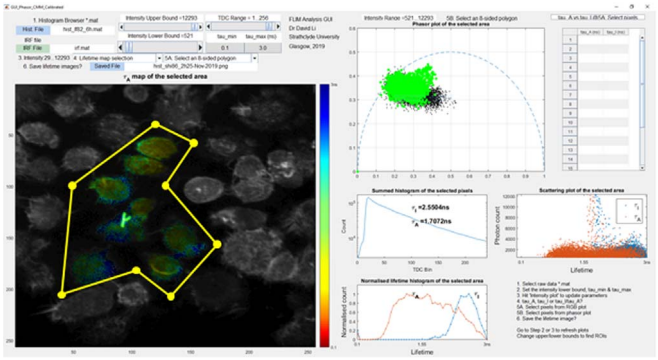

**Figure 1.** Newly developed platform for FLIM analysis showing highlighted lifetime images, phasor analysis, decay curves, lifetime histograms, and lifetime scattering plots corresponding to the selected region of interest (yellow line).

two-dimensional images at various depths of the cell, and it is possible to reconstruct to high-resolution 3D images. It is, however, a lengthy process, thus increasing the likelihood of cellular changes occurring.

FLIM provides contrast according to the fluorescence decay time and has been proven to be a powerful method in multi-labelled cell imaging [6–8]. It can be integrated with a confocal microscope or two-photon excitation microscope. In contrast to fluorescence intensity, the fluorescence decay time is independent of the local concentration of fluorophores, photobleaching, the local excitation intensity and local fluorescence detection efficiency. Moreover, the fluorescence decay times of aromatic molecules often depend on their intrinsic characteristics and local environments [9] such as $Ca^{2+}$ [10, 11], pH [12], viscosity [13], temperature [14], refractive index [15], or interactions with other molecules, such as collisional, quenching or energy transfer processes [16, 17]. Therefore, FLIM is not only able to distinguish spectrally overlapping fluorophores, but it can also be used to probe the immediate surroundings and dynamical processes of fluorophores. For example, previously intra-cellular imaging of gold nanorods using FLIM has shown improved contrast over fluorescence intensity imaging which results from large fluorescence lifetime differences; gold nanorods have typically short lifetimes (100 ps) compared to the fluorescence lifetimes of typical fluorophores (1.0 ∼ 4.0 ns) [18]. Furthermore, FLIM imaging can assess the energy transfer between gold nanorods to adjacent fluorophores, and FRET-FLIM has been successfully employed in resolving the cell take-up of gold nanorods and intracellular pathways [19, 20].

Commercially available FLIM analysis tools usually provide initial quick analysis such as first moment analysis, and curve-fitting routines for further detailed analysis that requires end-users to choose fitting models (mono-, bi- or multi-exponential) and perform the analysis based on whether the reduced-chi squared is within a specific user-selected criterion. Such exponential models, however, cannot be defined properly in complex biological systems and the fitting routine is not mathematically unique, which can lead to ambiguous interpretations. This is why more and more FLIM researchers are applying the phasor approach [11, 21, 22] to avoid complications in analysis and interpretations. Although some commercial tools do allow users to choose the areas of interest [23, 24], they are not free. The IRF is determined by the laser, the detector and the temporal dispersion of the time-correlated single-photon counting (TCSPC) electronics used in FLIM experiments. To avoid complications, traditional software tools might use a synthesized IRF to perform the analysis if the IRF is not available or measured beforehand. In this paper, we aim to report a new analysis platform that is model-fitting free based on newly developed algorithms that unlocks the limitations of fitting routines, therefore we can directly calculate fluorescence lifetimes without resolving all parameters. We will combine the proposed analysis methods with the phasor analysis. Users are able to choose regions of interests from either lifetime images or phasor plots and perform cross comparison studies for easy and rapidly differentiating intracellular, extracellular and membrane-bounded bacteria of diverse species. The platform is envisaged to facilitate studies on bacteria-host interactions. The innovative aspects of this work include:

1. Fluorescence lifetime is used as an indicator to locate intracellular bacteria to investigate the lifetime of bacteria at different cellular locations.
2. Experimental results showed that the proposed amplitude weighted lifetime analysis method is rapid and can provide better contrast in our research for identifying cellular locations of bacteria compared to other analysis models.
3. A new user-friendly platform for FLIM analysis has been developed (figure 1). The tool is able to A) analyse FLIM images with different lifetime models, B) allow users to pinpoint a cluster of pixels or identify lifetime populations through either phasor plots or lifetime images, and C) provide detailed lifetime distribution analysis.

## 2. Method

### 2.1. Cell preparation

The mouse raw macrophage cells were routinely cultured in DMEM (Dulbecco's Modified Eagle Medium) supplemented with 10% FCS (fetal calf serum) under 5% $CO_2$ at 37 °C. Cells were seeded on to glass coverslips in 24-well plates and cultured overnight for bacterial infection. Bacteria, which were engineered to express GFP (green fluorescent protein), were harvested from an early exponential phase and added to the cells with an MOI (multiplicity of infection) = 100. After 40–60 min incubation, extracellular bacteria were removed by washing 3 times with PBS (phosphate-buffered saline). Fresh DMEM supplemented with 50 $\mu$g ml$^{-1}$ of gentamicin was added to the cells for further incubation. At indicated time intervals cells were washed 3 times with PBS and fixed with 3.7% paraformaldehyde for 15 min. Cells were washed 3 times with PBS and permeabilized with 0.1% triton X-100 for 5 min. Cells were washed 3 times with PBS and stained for actin with phalloidin Alexa Flour 546 (ThermoFisher). The coverslips were then mounted for microscopy with a ProLong antifade solution (ThermoFisher).

### 2.2. Fluorescence intensity and lifetime imaging microscopy

FLIM was performed by using a confocal microscope (LSM510, Carl Zeiss) equipped with a time-correlated single-photon counting (TCSPC) module (SPC-830, Becker & Hickl GmbH). For z-stack imaging, an Argon laser of 488 nm was used as the single-photon excitation source and fluorescence emission was collected using a 500–550 nm bandpass filter for GFP labelled bacteria and a 565–615 nm bandpass filter for Alexa Fluor 548 labelled cell actin. A femtosecond Ti: Sapphire laser (Chameleon, Coherent) at 850 nm was used as a two-photon excitation source for FLIM imaging. The laser pulse has an 80 MHz repetition rate and a duration less than 200 fs. The emitted photons were collected through a 63× water-immersion objective lens (N.A. = 1.0) and a 500–550 nm bandpass filter. FLIM data were acquired through the non-descaned mode.

### 2.3. FLIM analysis

FLIM images were analysed by the platform using three different lifetime analysis: (1) amplitude weighted lifetime model ($\tau_A$), (2) intensity weighted lifetime model ($\tau_I$) and (3) mono-exponential fitting using commercial software ($\tau_C$). The decay function was calibrated by the IRF obtained from the measurement of dried urea ($(NH_2)_2CO$) [25]. The measured IRF or the synthesized IRF calculated from the rising edge of the fluorescence signal was used in $\tau_C$ analysis [26]. For the first two methods, we use a simple model to explain how the proposed analysis models work. Assume the true decay function, $f(t)$, to be estimated from the measured decay $y(t)$ and the measured IRF, $IRF(t)$, can be expressed as

$$f(t) = \sum_{i=1}^{p} a_i e^{-\frac{t}{\tau_i}} \tag{1}$$

where $a_i$ is the amplitude and $\tau_i$ is the lifetime of the $i$th species, i = 1,…, $p$, $\sum_i^p a_i = 1$, and $p$ is the number of lifetime species. Traditional FLIM analysis tools usually apply curve-fitting techniques to resolve $a_i$ and $\tau_i (i = 1, \ldots, p)$ from reconvolution

$$y(t) = f(t) \otimes IRF(t) \tag{2}$$

where $y(t)$ isthe measured fluorescence decayfunction. Solving this inverse problem to obtain the amplitude and lifetime components, however, is time-consuming and can be prone to errors and artefacts, especially when the photon count is low. In many applications, the analysis goals are to obtain the intensity weighted lifetime, $\tau_I$, or the amplitude-weighted lifetime, $\tau_A$, defined by [27]:

$$\tau_I = \frac{\sum_{i=1}^{p} a_i \tau_i^2}{\sum_{i=1}^{p} a_i \tau_i} \text{ or } \tau_A = \frac{\sum_{i=1}^{p} a_i \tau_i}{\sum_{i=1}^{p} a_i} \tag{3}$$

to provide contrast instead of resolving all unknown parameters. Without resorting to complex iterative curve-fitting routines, there are easier ways to estimate $\tau_I$ and $\tau_A$. The former has been proven [28] to be approximate to the centre-of-mass method without [29] or with the IRF considered [30], whereas the latter can be easily obtained as well with the IRF considered (the details will be reported separately). $\tau_I$ and $\tau_A$ are simply two different mappings, and they should be carefully used to optimise the contrast according to users' applications. In this study, we will demonstrate how they can be used to differentiate bacteria in extra- and intra-cellular or membrane-bounded locations. Note that when an amplitude is dominating ($a_i \sim 1.0$), then $\tau_I/\tau_A \sim 1.0$, meaning the measured decay for this pixel is nearly mono-exponential decay and on the phasor plot it is close to the unit circle. The measured IRF is also calibrated in the phasor analysis provided by the proposed analysis platform.

## 3. Results and discussion

### 3.1. Comparisons between three lifetime analysis models: $\tau_A$, $\tau_I$ and commercial software ($\tau_C$)

To disclose the locations of Shi86 with macrophage cells, z-stack fluorescence imaging was performed with each layer of 1 $\mu$m thickness. Internalization of bacteria in cells has been reported before and studied using z-stack confocal microscopy [31–33]. Figure 2 shows three slices of the z-stack images where Shi86 were labelled with their cellular locations identified, for example in figure 2(b), (A) extracellular, (B) intracellular, and (C) membrane-bounded where the bacteria are near the cell membrane. To identify these locations, 20 z-stack images were used. The

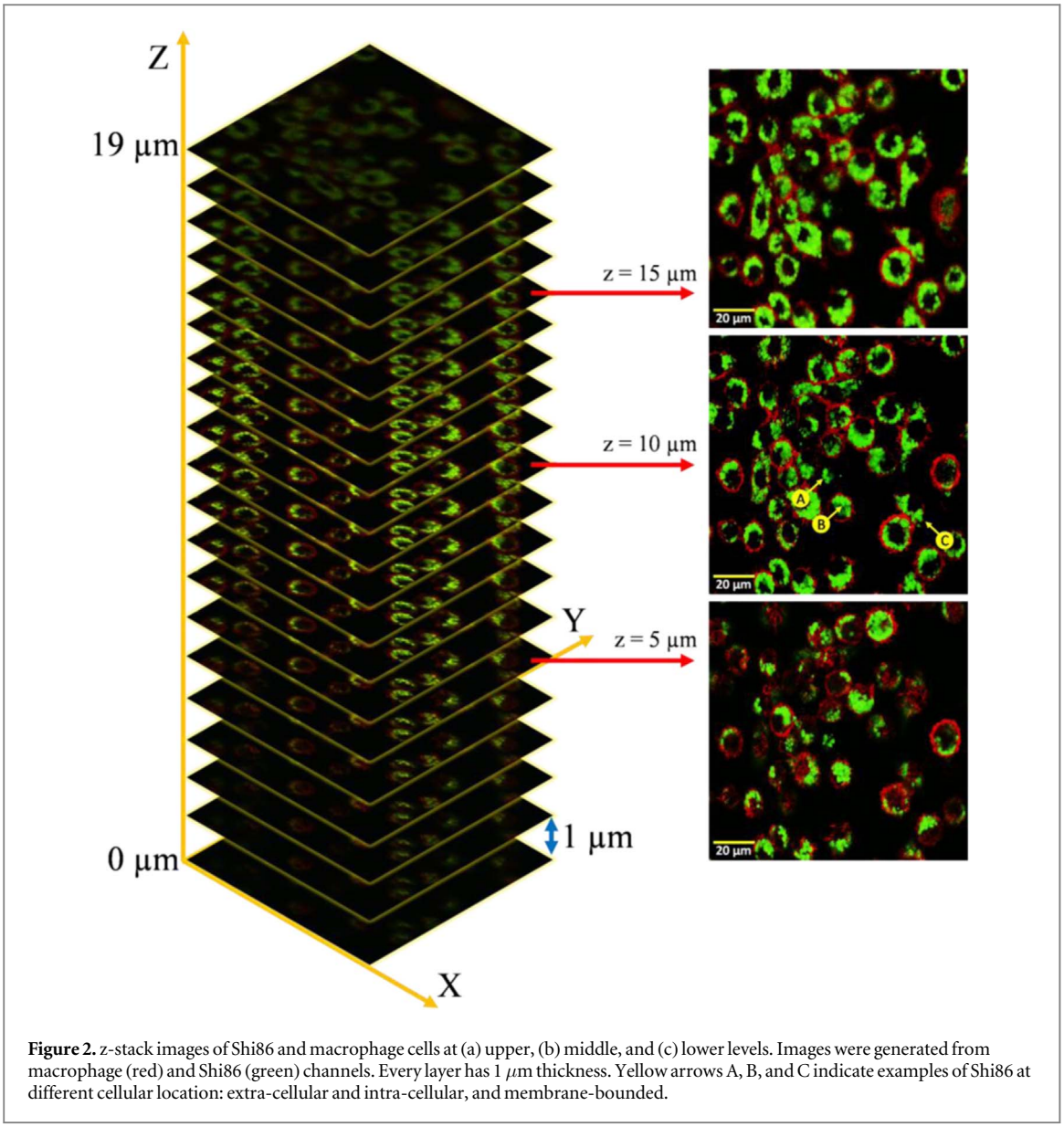


**Figure 2.** z-stack images of Shi86 and macrophage cells at (a) upper, (b) middle, and (c) lower levels. Images were generated from macrophage (red) and Shi86 (green) channels. Every layer has 1 $\mu$m thickness. Yellow arrows A, B, and C indicate examples of Shi86 at different cellular location: extra-cellular and intra-cellular, and membrane-bounded.

information obtained from z-stack images can be used for cross comparisons with two-photon FLIM images, such as the ones taken in the same area as figure 2(b).

Figure 3 shows fluorescence lifetimes of GFP labelled Shi86 at three different cellular locations (intracellular, membrane-bounded and extracellular) and Alexa Flour 546 from macrophage cells, respectively. 106 Shi86 were analysed, and the lifetime changes of GFP were found to be related to their cellular locations. $\tau_A$ analysis shows better contrast than the other models. This agrees well with the conclusions summarised in [28] that $\tau_A$ analysis is suitable for investigating different species showing subtle lifetime differences or for studying samples showing a small FRET efficiency. The mean lifetime of GFP and Alexa Fluor 546 was reported to be 2.00 ns [19, 34] and 2.59 ns [35]. The lifetime of Alexa Fluor 546 is found as the long lifetime component in the FLIM image with $\tau_A = 1.94 \pm 0.33$ ns, $\tau_I = 2.50 \pm 0.08$ ns and $\tau_C = 2.81 \pm 0.15$ ns, respectively. $\tau_A$ indicates significant lifetime differences that the intracellular Shi86 has a relatively short lifetime ($\tau_A = 1.34 \pm 0.30$ ns), and the extracellular Shi86 shows a long lifetime ($\tau_A = 1.76 \pm 0.32$ ns), however, the Shi86 at the membrane-bounded location ($\tau_A = 1.46 \pm 0.26$ ns) is insignificantly different to intracellular Shi86. $\tau_I$ has the highest precision and the same trends as $\tau_A$ and $\tau_C$, however, it shows the least contrast. The $\tau_I$ analysis of intracellular, membrane-bounded and extracellular Shi86 shows $\tau_I = 2.07 \pm 0.11$ ns, $\tau_I = 2.14 \pm 0.11$ ns and $\tau_I = 2.28 \pm 0.14$ ns, whereas $\tau_C$ model obtains $\tau_C = 2.09 \pm 0.15$ ns, $\tau_C = 2.12 \pm 0.11$ ns and $\tau_C = 2.18 \pm 0.11$ ns. $\tau_C$ analysis can also provide results calibrated with the measured IRF, giving $\tau_{C(IRF)} = 1.72 \pm 0.06$ ns, $\tau_{C(IRF)} = 1.83 \pm 0.06$ ns, $\tau_{C(IRF)} = 1.97 \pm 0.37$ ns, respectively.

The tool allows users to set intensity thresholds to remove pixels with insufficient photon counts, for example, the pixels mainly collecting dimmer autofluorescence.

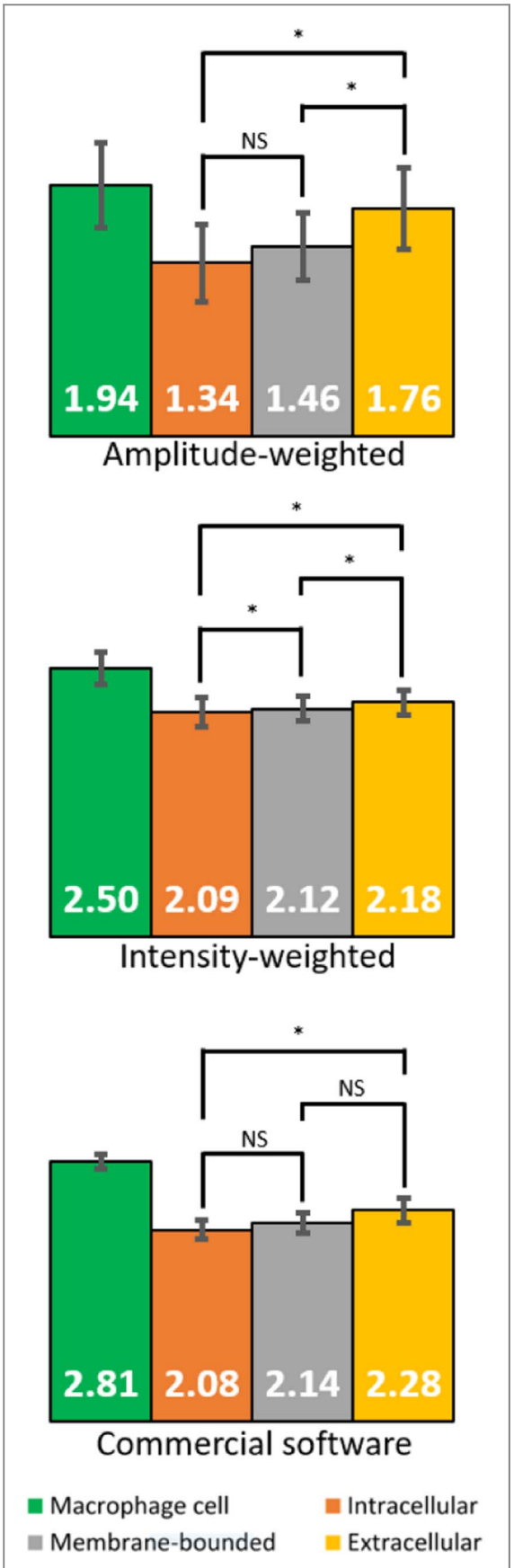


**Figure 3.** Average fluorescence lifetimes of macrophage and Shi86 at different cellular locations analysed by three different models: $\tau_A$, $\tau_I$ and $\tau_C$, where * = p > 0.05 and NS = non-significant.

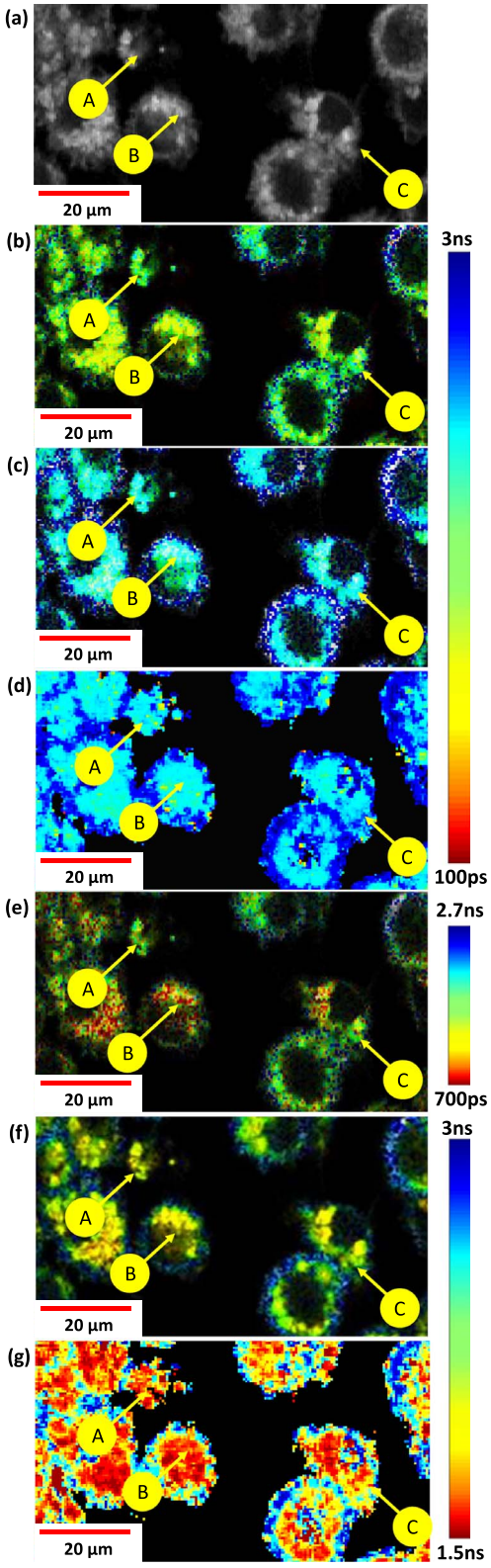


**Figure 4.** Images generated by the developed platform including (a) Two-photon luminescence intensity and (b), (c) and (d) are $\tau_A$, $\tau_I$ and $\tau_C$ images of Shi86 together with macrophage, respectively with the colour scale 0.1 ns to 3 ns. (e) $\tau_A$ image with the colour scale 0.7 to 2.7 ns. (f) and (g) are $\tau_I$ and $\tau_C$ images with the colour scale 1.5 ns to 3 ns respectively. Yellow arrows A, B, and C indicate examples of Shi86 at different cellular location: extra-cellular and intra-cellular, and membrane-bounded.

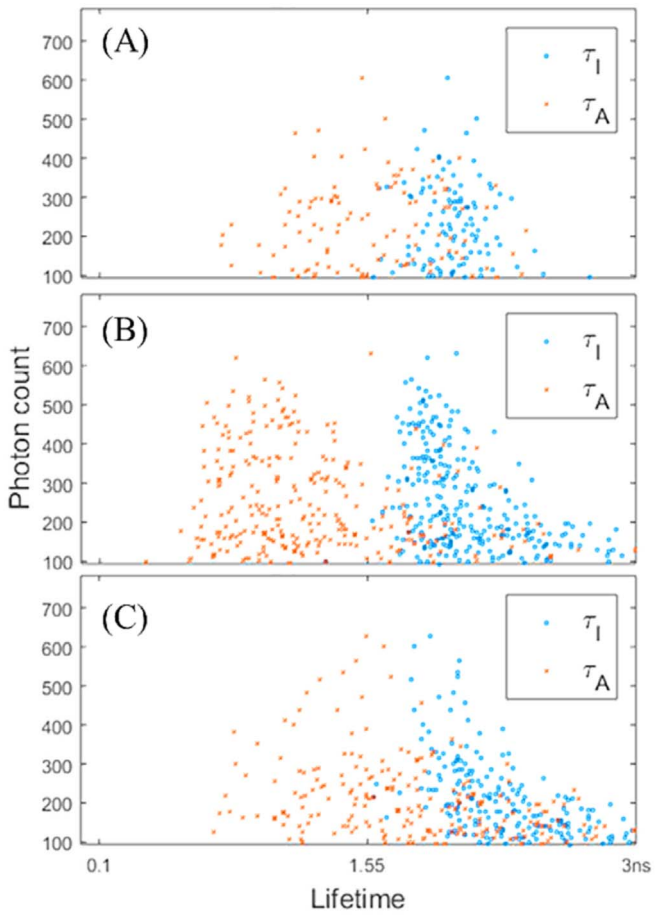


**Figure 5.** Photon counts and fluorescence lifetime plot of position (A), (B) and (C) in figure 4.

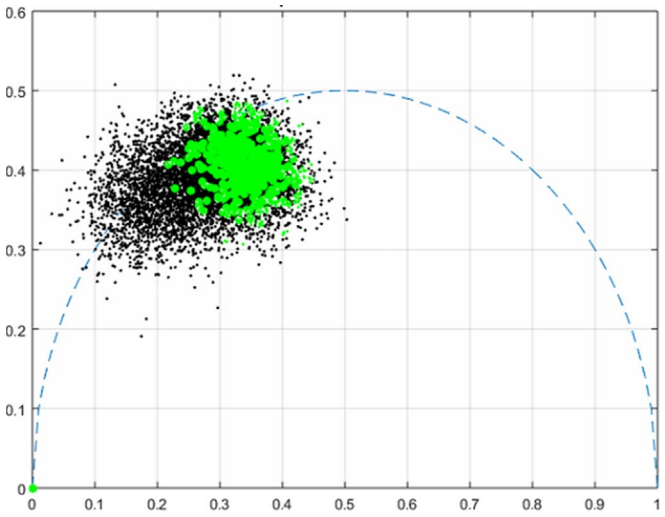

**Figure 6.** Phasor plot of figure 4 showing two lifetime populations: Shi86 (green) and macrophage (black).

The threshold was set to be above 100 photons for each pixel, as our $\tau_A$ and $\tau_I$ analysis models require a less photon count than what multi-exponential fitting methods do [28]. Figures 5(a)–(c) shows scattering plots of the photon count versus the lifetime for both models. It clearly indicates that $\tau_A$ offers better differentiation to bacterial cellular locations, compared to $\tau_I$.

Figures 4(b), (c), (e) and (f) are FLIM images generated by the developed platform where the black areas mean the pixels outside the interested intensity range. Figure 4(a) is a two-photon luminescence intensity image and figures 4(b)–(d) are initial $\tau_A$, $\tau_I$, and $\tau_C$ images showing Shi86 and macrophage cells obtained from the same area as figure 2(b), respectively. Figure 4(b) is

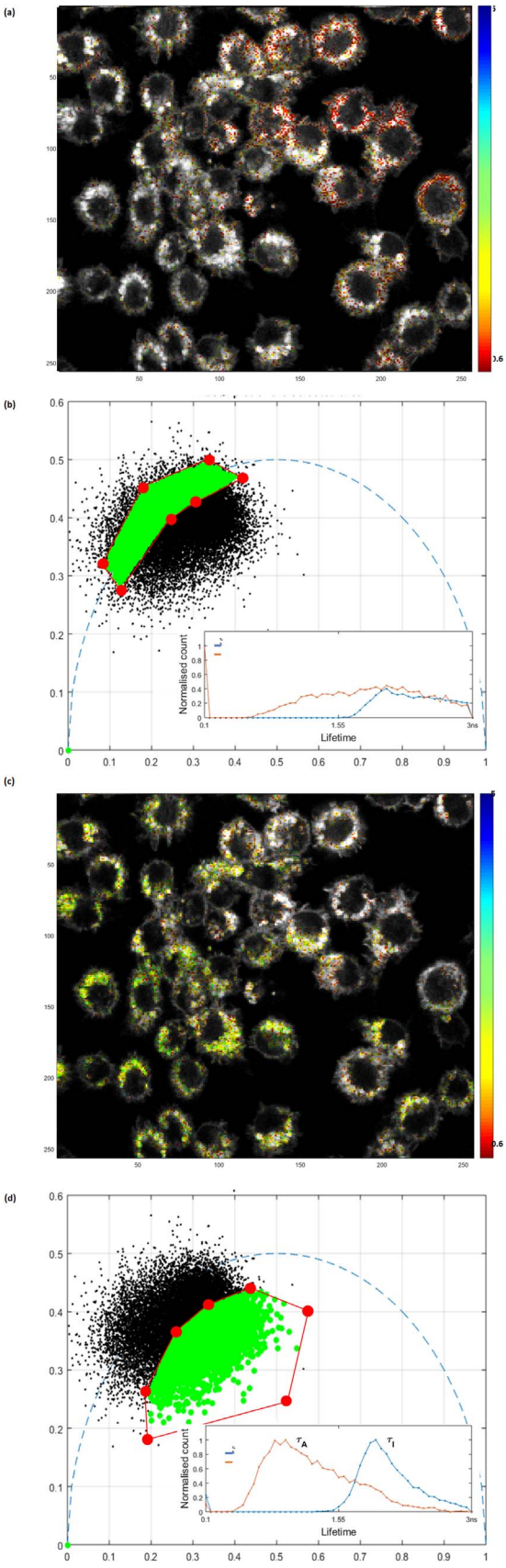


**Figure 7.** (a) and (c) Colour-coded $\tau$I/$\tau$A images for the regions of interest encircled in (b) and (d) phasor plots, respectively. (b) and (d) also show the corresponding lifetime histograms. Grey scale pixels mean the pixels outside the selected areas.

the $\tau_A$ image, and it reveals multi coded colours of Shi86 depending on their cellular locations, whereas $\tau_I$ and $\tau_C$ provide lower contrast. Shi86 are obvious in figure 4(b) but are not clear in the intensity image (figure 4(a)). Figures 4(e)–(g) are the same image as figures 4(b)–(d), but with different colour scales, 0.7–2.7 ns for (e) and 1.5–3.0 ns for (f) and (g), showing better contrast. It is, however, still difficult to distinguish the cellular positions of bacteria due to the subtle differences in coded lifetimes for figures 4(c), (d), (f) and (g). Moreover, the phasor plot (figure 6) was used to distinguish populations in the lifetime image presenting clearly two clusters: Shi86 and macrophage.

In addition, the locations of bacteria can be investigated by observing the ratio of $\tau_I/\tau_A$. Both models give similar lifetimes of the extracellular Shi86, which makes the ratio $\tau_I/\tau_A$ closer to 1. However, the ratio increases during phagocytosis because $\tau_I$ and $\tau_A$ of intracellular Shi86 are significantly different. Therefore, the ratio $\tau_I/\tau_A$ can improve the contrast, a good indicator to reveal the locations of bacteria. Figures 7(a) and (c) show $\tau_I/\tau_A$ images in the same area as figure 2(b) with the ratio analysis that relates to the position in the phasor plot, while figures 7(b) and (d) are their interest encircled phasor plot, respectively. In figure 7(b), the selected area is close to the semi-circle encircled by the 8-sided polygon defined by the user. This area includes some parts related to the cell membrane and extracellular Shi86 with an average ratio = 1.19. In contrast, figure 7(d) shows the area that covers inside the semi-circle with an average ratio of 1.69. This area covers mostly the intracellular Shi86.

### 3.2. Applying $\tau_A$ model to other types of bacteria

Since $\tau_A$ has shown to have better contrast compared with the other two models in the case of *S. sonnei,* we applied this model to analyse Raw cells infected by other bacteria: AIEC strains HM605 and HH427, and a *Lactobacillus* strain. Figure 8 shows $\tau_A$ images, which were generated using the same conditions as above. The arrows indicate the bacteria. As in the example for Shi86, the $\tau_A$ model adequately differentiated intracellular, extracellular and membrane-bounded bacteria in all cases (table 1). Table 1 includes $\tau_C$ analysis results using the synthesized and measured IRFs, but they do not show obvious differences. Traditional analysis tools usually use least square fitting routines to perform model-fitting analysis. For mono-exponential analysis, the fitting routine usually generates results close to $\tau_I$ analysis [36]. This is in good agreement with what we obtained from table 1. $\tau_A$ shows the potential to differentiate cellular locations of bacteria. Extracellular HM605, HH427 and *Lactobacillus* have luminescence lifetimes of 1.84 ± 0.03 ns, 1.73 ± 0.21 ns and 1.33 ± 0.17 ns, respectively, whereas the intracellular bacteria have obviously shorter lifetimes of

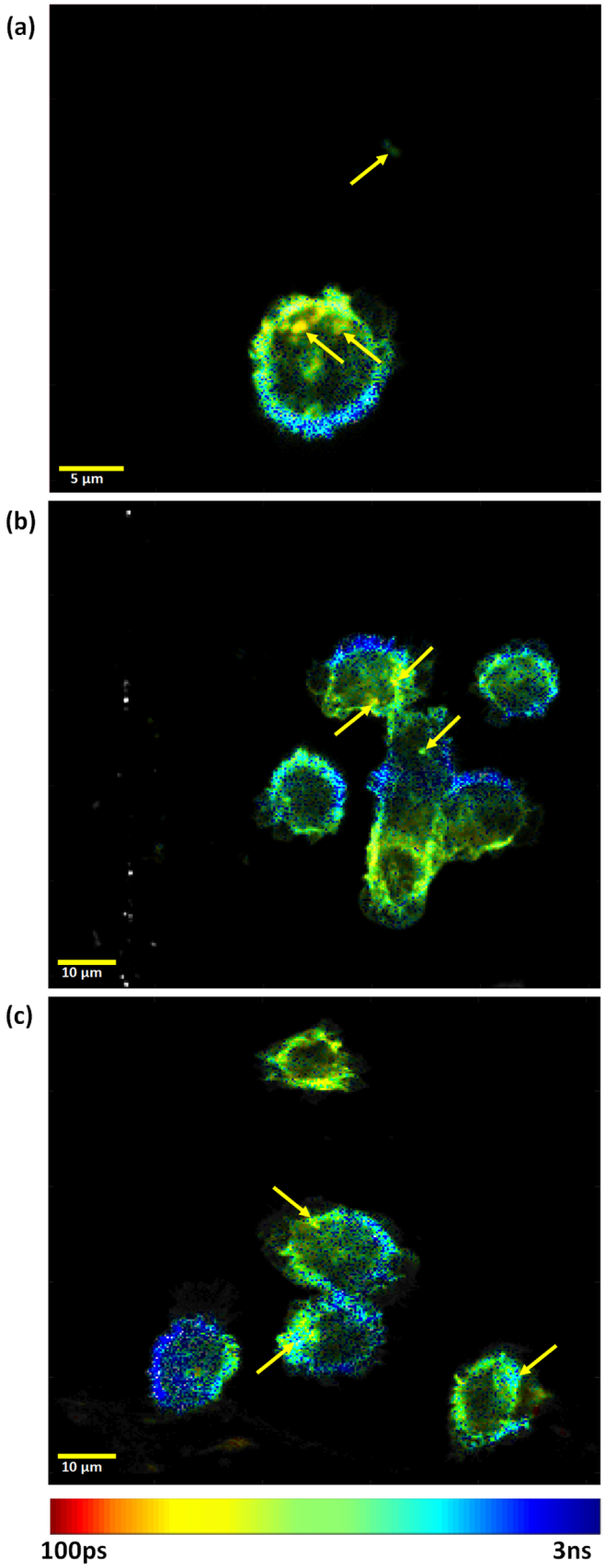


**Figure 8.** $\tau$A images of macrophage cells treated with (a) HH427, (b) HM605 and (c) lactobacillus. Yellow arrows indicate the locations of bacteria.

**Table 1.** Fluorescence lifetimes of HM605, HH427 and *Lactobacillus* at the different cellular location where E, M and I mean extra-cellular, membrane-bounded and intra-cellular.

| Bacteria and Location | | Fluorescence lifetime (ns) | | | |
|---|---|---|---|---|---|
| | | $\tau_A$ | $\tau_I$ | $\tau_C$ | $\tau_{C(IRF)}$ |
| HM 605 | E | 1.84 ± 0.03 | 2.41 ± 0.14 | 2.17 ± 0.12 | 2.18 ± 0.11 |
| | M | 1.51 ± 0.15 | 2.51 ± 0.09 | 2.42 ± 0.05 | 2.38 ± 0.09 |
| | I | 1.52 ± 0.10 | 2.28 ± 0.05 | 2.33 ± 0.07 | 2.33 ± 0.07 |
| HH 427 | E | 1.73 ± 0.21 | 2.32 ± 0.30 | 2.25 ± 0.26 | 2.20 ± 0.23 |
| | M | 1.62 ± 0.25 | 2.42 ± 0.17 | 2.38 ± 0.14 | 2.42 ± 0.01 |
| | I | 1.66 ± 0.42 | 2.37 ± 0.14 | 2.34 ± 0.13 | 2.28 ± 0.12 |
| *Lactobacillus* | E | 1.33 ± 0.17 | 2.11 ± 0.13 | 2.20 ± 0.09 | 2.12 ± 0.10 |
| | M | 1.04 ± 0.13 | 2.13 ± 0.19 | 2.12 ± 0.06 | 2.16 ± 0.05 |
| | I | 1.18 ± 0.05 | 2.28 ± 0.12 | 2.18 ± 0.18 | 2.12 ± 0.03 |

1.52 ± 0.10 ns, 1.66 ± 0.42 ns and 1.18 ± 0.05 ns, respectively. Membrane-bounded bacteria also have similar lifetimes (as the intracellular bacteria) of 1.51 ± 0.15 ns, 1.62 ± 0.25 ns and 1.04 ± 0.13 ns for HM605, HH427 and *Lactobacillus*, respectively.

This indicates that the lifetime of GFP labelled bacteria is shorter during internalization processes. However, $\tau_I$ and $\tau_C$ are not as effectively as $\tau_A$ to distinguish the cellular locations of bacteria, and we will conduct more imaging experiments to investigate this further.

In summary, we have built an effective platform, which can rapidly identify cellular locations of facultative intracellular bacteria. Both models ($\tau_A$ and $\tau_I$) have speedy performances and superior clarity than intensity imaging and are theoretically faster than traditional fitting methods, as our models do not require model selections or require setting extra constraints as most traditional analysis tools do [26]. Our tool only takes 0.3 s to generate $\tau_A$ images or 0.1 s (comparable to the speed of the first moment analysis of commercial software tools at 10 fps [37]) for $\tau_I$ images with 2.8 GHz Intel Core i7 processor. Moreover, our direct estimation algorithms are hardware-friendly, offering even much faster analysis if they are implemented in electronics hardware [29, 38]. Although commercial software tools might also provide $\tau_A$ and $\tau_I$ analysis functions, they usually need to perform multi-exponential fitting routines to extract all necessary parameters first and then use equation (3) to obtain $\tau_A$ or $\tau_I$ [23, 24]. Moreover, the proposed tool offers extra analysis functions ($\tau_A$, $\tau_I$ and $\tau_I/\tau_A$), whereas fitting methods that have been used in most free tools only provide close-to-$\tau_I$ analysis [39, 40]. Different tools provide their own strategies of selecting areas of interest, but they do not offer comparable speedy analysis. Although some commercial tools are also user-friendly to allow users choosing their areas of interest [23, 24], they are unfortunately not free.

The $\tau_A$ model has the best contrast and this is suitable for quick imaging samples with unknown lifetimes, investigating samples with subtle lifetime differences (in this study to investigate intracellular, extracellular and membrane-bounded bacteria) or imaging samples showing a small FRET efficiency. Although, the $\tau_I$ has shown excellent precision and small deviations for Shi86 and is suitable for further imaging applications that require higher precision or a higher signal-to-noise ratio. Users are able to choose the proper indicator for their applications. From the experiments and the analysis conducted, this platform holds a high potential to identify the locations of bacteria from their lifetimes without performing z-stack imaging. The imaging platform, as well as the tool developed, can be widely applied by researchers conducting FLIM measurements. Researchers interested in this tool are welcome to contact the corresponding author Dr David Li (David.Li@strath.ac.uk). The analysis tool and future updates will be available to the public through Strathclyde Pure.

## Acknowledgments

N. Sapermsap acknowledges the Development and Promotion of Science and Technology Talents (DPST) Project under the Institute for the Promotion of Teaching Science and Technology (IPST), Thailand, for a PhD scholarship. This work was also supported by Medical Research Scotland (PhD-1179–2017) and the QuantIC EPSRC Quantum Technology Hub. Yahui Li contributed to the optimisation of the tool, and her study has been supported by the China Scholarship Council. The authors have declared that no conflicting interests exist.

## ORCID iDs

Natakorn Sapermsap https://orcid.org/0000-0003-3268-0576
David Day-Uei Li https://orcid.org/0000-0002-6401-4263
David JS Birch https://orcid.org/0000-0001-6400-1270
Yu Chen https://orcid.org/0000-0003-2427-3559

## References


[1] Welling M M, Hensbergen A W, Bunschoten A, Velders A H, Scheper H, Smits W K, Roestenberg M and van Leeuwen F W B 2019 Fluorescent imaging of bacterial infections and recent advances made with multimodal radiopharmaceuticals *Clin. Transl. Imaging* **7** 125–38

[2] Rennie M Y, Dunham D, Lindvere-Teene L, Raizman R, Hill R and Linden R 2019 Understanding real-time fluorescence signals from bacteria and wound tissues observed with the MolecuLight i:X$^{TM}$ *Diagnostics (Basel, Switzerland)* **9** 22

[3] Szaszák M, Steven P, Shima K, Orzekowsky-Schröder R, Hüttmann G, König I R, Solbach W and Rupp J 2011 Fluorescence lifetime imaging unravels C. trachomatis metabolism and its crosstalk with the host cell *PLoS Pathog.* **7** e1002108

[4] Bhattacharjee A, Datta R, Gratton E and Hochbaum A I 2017 Metabolic fingerprinting of bacteria by fluorescence lifetime imaging microscopy *Sci. Rep.* **7** 3743

[5] Pedretti E *et al* 2019 High-speed dual color fluorescence lifetime endomicroscopy for highly-multiplexed pulmonary diagnostic applications and detection of labeled bacteria *Biomed. Opt. Express* **10** 181–95

[6] Becker W 2012 Fluorescence lifetime imaging—techniques and applications *J. Microsc.* **247** 119–36

[7] Suhling K *et al* 2015 Fluorescence lifetime imaging (FLIM): basic concepts and some recent developments *Med. Photonics* **27** 3–40

[8] Meyer-Almes F-J 2017 Fluorescence lifetime based bioassays *Methods. Appl. Fluoresc.* **5** 42002

[9] Berezin M Y and Achilefu S 2010 Fluorescence lifetime measurements and biological imaging *Chem. Rev.* **110** 2641–84

[10] Zheng K, Jensen T P and Rusakov D A 2018 Monitoring intracellular nanomolar calcium using fluorescence lifetime imaging *Nat. Protoc.* **13** 581

[11] Celli A, Sanchez S, Behne M, Hazlett T, Gratton E and Mauro T 2010 The epidermal Ca(2+) gradient: measurement using the phasor representation of fluorescent lifetime imaging *Biophys. J.* **98** 911–21

[12] Orte A, Alvarez-Pez J M and Ruedas-Rama M J 2013 Fluorescence lifetime imaging microscopy for the detection of intracellular pH with quantum dot nanosensors *ACS Nano* **7** 6387–95

[13] Battisti A, Panettieri S, Abbandonato G, Jacchetti E, Cardarelli F, Signore G, Beltram F and Bizzarri R 2013 Imaging intracellular viscosity by a new molecular rotor suitable for phasor analysis of fluorescence lifetime *Anal. Bioanal. Chem.* **405** 6223–33

[14] Okabe K, Inada N, Gota C, Harada Y, Funatsu T and Uchiyama S 2012 Intracellular temperature mapping with a fluorescent polymeric thermometer and fluorescence lifetime imaging microscopy *Nat. Commun.* **3** 705–9

[15] van Manen H-J, Verkuijlen P, Wittendorp P, Subramaniam V, van den Berg T K, Roos D and Otto C 2008 Refractive index sensing of green fluorescent proteins in living cells using fluorescence lifetime imaging microscopy *Biophys. J.* **94** L67–9

[16] Lakowicz J R 2006 *Principles of Fluorescence Spectroscopy* 3rd edn (New York: Springer)

[17] Fruhwirth G O *et al* 2011 How Förster resonance energy transfer imaging improves the understanding of protein interaction networks in cancer biology *ChemPhysChem* **12** 442–61

[18] Zhang Y, Yu J, Birch D J S and Chen Y 2010 Gold nanorods for fluorescence lifetime imaging in biology *J. Biomed. Opt.* **15** 020504

[19] Zhang Y, Wei G, Yu J, Birch D J S and Chen Y 2015 Surface plasmon enhanced energy transfer between gold nanorods and fluorophores: application to endocytosis study and RNA detection *Faraday Discuss.* **178** 383–94

[20] Zhang Y, Birch D J S and Chen Y 2011 Two-photon excited surface plasmon enhanced energy transfer between DAPI and gold nanoparticles: opportunities in intra-cellular imaging and sensing *Appl. Phys. Lett.* **99** 103701

[21] Digman M A, Caiolfa V R, Zamai M and Gratton E 2008 The phasor approach to fluorescence lifetime imaging analysis *Biophys. J.* **94** 14–6

[22] Basuki J S, Duong H T T, Macmillan A, Erlich R B, Esser L, Akerfeldt M C, Whan R M, Kavallaris M, Boyer C and Davis T P 2013 Using fluorescence lifetime imaging microscopy to monitor theranostic nanoparticle uptake and intracellular doxorubicin release *ACS Nano* **7** 10175–89

[23] Trautmann S, Buschmann V, Orthaus S, Koberling F, Ortmann U and Erdmann R 2013 Fluorescence lifetime imaging (FLIM) in confocal microscopy applications: an overview *Application Note* (https://picoquant.com/images/uploads/page/files/7350/appnote_flim_overview.pdf)

[24] Hille C, Lahn M and Dosche C 2008 Two-photon fluorescence lifetime imaging (2P-FLIM) for ion sensing in living cells *Application Note* (https://picoquant.com/images/uploads/page/files/7269/appnote_twophotonexcitation.pdf)

[25] Becker W 2008 Recording the instrument response function of a multiphoton FLIM system *Application Note* (https://becker-hickl.com/wp-content/uploads/2018/12/irf-mp-v04.pdf)

[26] Becker W 2017 *The bh TCSPC Handbook* 7th edn (Berlin: Becker & Hickl GmbH)

[27] Sillen A and Engelborghs Y 1998 The correct use of 'average' fluorescence parameters *Photochem. Photobiol.* **67** 475–86

[28] Li D D U, Ameer-Beg S, Arlt J, Tyndall D, Walker R, Matthews D R, Visitkul V, Richardson J and Henderson R K 2012 Time-domain fluorescence lifetime imaging techniques suitable for solid-state imaging sensor arrays *Sensors (Switzerland)* **12** 5650–69

[29] Li D U *et al* 2011 Video-rate fluorescence lifetime imaging camera with CMOS single-photon avalanche diode arrays and high-speed imaging algorithm *J. Biomed. Opt.* **16** 096012

[30] Poland S P *et al* 2016 New high-speed centre of mass method incorporating background subtraction for accurate determination of fluorescence lifetime *Opt. Express* **24** 6899–915

[31] Knodler L A, Vallance B A, Celli J, Winfree S, Hansen B, Montero M and Steele-Mortimer O 2010 Dissemination of invasive Salmonella via bacterial-induced extrusion of mucosal epithelia *Proc. Natl. Acad. Sci. U. S. A.* **107** 17733–8

[32] Capasso D, Pepe M V, Rossello J, Lepanto P, Arias P, Salzman V and Kierbel A 2016 Elimination of pseudomonas aeruginosa through efferocytosis upon binding to apoptotic cells *PLoS Pathog.* **12** e1006068

[33] Kjos M, Aprianto R, Fernandes V E, Andrew P W, Van Strijp J A G, Nijland R and Veening J W 2015 Bright fluorescent streptococcus pneumoniae for live-cell imaging of host-pathogen interactions *J. Bacteriol.* **197** 807–18

[34] Li W, Houston K D and Houston J P 2017 Shifts in the fluorescence lifetime of EGFP during bacterial phagocytosis measured by phase-sensitive flow cytometry *Sci. Rep.* **7** 1–11

[35] Askari J A, Tynan C J, Webb S E D, Martin-Fernandez M L, Ballestrem C and Humphries M J 2010 Focal adhesions are sites of integrin extension *J. Cell Biol.* **188** LP–903

[36] Fišerová E and Kubala M 2012 Mean fluorescence lifetime and its error *J. Lumin.* **132** 2059–64

[37] Liu X, Lin D, Becker W, Niu J, Yu B, Liu L and Qu J 2019 Fast fluorescence lifetime imaging techniques: a review on challenge and development *J. Innov. Opt. Health Sci.* **12** 1930003

[38] Li D-U, Arlt J, Richardson J, Walker R, Buts A, Stoppa D, Charbon E and Henderson R 2010 Real-time fluorescence lifetime imaging system with a 32 × 32 0.13 $\mu$m CMOS low dark-count single-photon avalanche diode array *Opt. Express* **18** 10257–69

[39] Kim J, Tsoy Y, Persson J and Grailhe R 2017 FLIM-FRET analyzer: open source software for automation of lifetime-based FRET analysis *Source Code Biol. Med.* **12** 7

[40] Warren S C, Margineanu A, Alibhai D, Kelly D J, Talbot C, Alexandrov Y, Munro I, Katan M, Dunsby C and French P M W 2013 Rapid global fitting of large fluorescence lifetime imaging microscopy datasets *PLoS One* **8** e70687